EurJIC
European Journal of Inorganic Chemistry

Research Article
doi.org/10.1002/ejic.202300784

Chemistry Europe
European Chemical Societies Publishing

www.eurjic.org

Structural, stability and relaxation features of lanthanide-complexes designed for multimodal imaging detection of enzyme activities

Sophie Laine,[a] Rémy Jouclas,[b] Célia S. Bonnet,[a] Pascal Retailleau,[b] Vincent Steinmetz,[b] Agnès Pallier,[a] Zoltán Garda,[a, c] Gyula Tircsó,*[c] Philippe Durand,*[b] and Éva Tóth*[a]

Lanthanide complexes of DO3A-derivative ligands bearing a pyridine-carbamate (**L1**) or pyridine-amine (**L2**) arm have potential interest in the design of enzymatically activated imaging probes. Solid-state X-ray structures for **CeL1** and **YbL2** both demonstrate twisted square antiprismatic geometry, with the metal ion in a nine- or an eight-coordinate environment, respectively. As assessed by pH-potentiometry, in solution lanthanide ions form more stable complexes with the non-adentate **L1** than with the octadentate **L2** ligand ($\log K_{ML} = 18.7–21.1$ vs. 16.7–18.6, respectively), while stability constants are similar for L1 and L2 chelates of Mg^{2+}, Ca^{2+}, Zn^{2+} or Cu^{2+}. The kinetic inertness of **GdL1** is exceptionally high, with an estimated dissociation half-life of ~10^8 h at pH 7.4, while **LnL2** (Ln=Ce, Gd, Yb) complexes have 3–4 orders of magnitude faster dissociation, related to the presence of the protonatable, non-coordinating amine function. The water exchange rate determined for the monohydrated **GdL2** ($k_{ex}^{298} = 1.3\times10^6\ s^{-1}$) shows a threefold decrease with respect to GdDOTA, as a consequence of a reduction in the negative charge and in the steric crowding around the water binding site, both important in dissociatively activated water exchange processes.

Introduction

Thanks to its excellent spatial resolution and the lack of ionizing radiation, Magnetic Resonance Imaging (MRI) has become the most prominent full body imaging modality in the clinics. In MRI, Gd^{3+} complexes are commonly used to improve image contrast.[1–2] Following intravenous injection, these paramagnetic chelates distribute into extracellular spaces and shorten the relaxation times, T_1 and T_2, of water proton nuclei in the surrounding tissue. While today all commercial contrast agents are non-specific, enormous research efforts have been made in the last two decades towards the development of Gd^{3+} chelates which can allow for the specific detection of biologically relevant biomarkers.[3–5] Such responsive or smart probes are capable of specifically changing their relaxation properties upon interaction with a specific biomarker, with a concomitant variation of signal intensity in the MR images.

In addition to classical MRI based on the detection of nuclear relaxation properties of tissue (mainly water) protons, chemical exchange saturation transfer (CEST) has emerged more recently as an alternative mechanism to create MR images.[6] CEST contrast agents possess protons in slow exchange with surrounding water protons. Due to the exchange, selective irradiation of these slowly exchanging protons on their NMR resonance frequencies will lead to a signal intensity decrease of the bulk water protons as a result of spin exchange, which can be translated to an MR image. Paramagnetic shift reagents, often based on lanthanide complexes, are commonly used as CEST probes, inducing greater separation between the probe and the water resonance frequencies.[7–8] This facilitates selective irradiation and allows for the exploitation of faster proton exchange rates while remaining in the slow exchange regime, leading to higher CEST effects.

Enzymes represent an important class of imaging biomarkers, since many pathological states are directly associated with their misregulation. A high number of enzymatically activated MRI probes have been reported in the past, including both relaxation agents based on Gd^{3+} and PARACEST probes based on other lanthanide ions, some of them have been successfully used in preclinical *in vivo* experiments as well.[9–13] It is generally considered that enzymatic detection can be well adapted to MRI. Indeed, enzymes work in catalytic cycles, thus even if present at low concentration, they are able to transform a large quantity of the contrast agent. This is particularly important considering the low sensitivity of MRI which typically requires ~10 μM local concentrations of the probe in order to

[a] Dr. S. Laine, Dr. C. S. Bonnet, A. Pallier, Dr. Z. Garda, Dr. É. Tóth
Center of Molecular Biophysics, CNRS UPR 4301
University of Orléans
rue Charles Sadron, 45071 Orléans, France
E-mail: eva.jakabtoth@cnrs-orleans.fr

[b] Dr. R. Jouclas, Dr. P. Retailleau, V. Steinmetz, Dr. P. Durand
Institut de Chimie des Substances Naturelles, CNRS UPR 2301
Université Paris-Saclay
1, av.de la Terrasse, 91198 Gif-sur-Yvette, France
E-mail: philippe.durand@cnrs.fr

[c] Dr. Z. Garda, Dr. G. Tircsó
Department of Physical Chemistry
University of Debrecen
Egyetem tér 1, 4010 Debrecen, Hungary
E-mail: gyula.tircso@science.unideb.hu

Supporting information for this article is available on the WWW under https://doi.org/10.1002/ejic.202300784

Research Article
doi.org/10.1002/ejic.202300784

be detected, preventing the visualization of many low-concentration biomarkers.

Although it is common knowledge that Ln^{3+} complexes designed for *in vivo* application need to have sufficient thermodynamic stability and kinetic inertness in order to avoid toxicity related to the release of free metal ions,[14] these properties are relatively rarely assessed for responsive contrast agents. Such studies are particularly important when the interaction of the lanthanide chelate with the biomarker implies changes in the coordination sphere of the metal ion, which can have direct consequences on the stability and the inertness of the complex. Indeed, for Gd^{3+}-based responsive probes, the relaxivity change induced by the biomarker is very often related to a change in the hydration number of the metal ion, resulting from the coordination or de-coordination of one (or more) donor groups of the ligand.[5] This will obviously have a strong impact on the thermodynamic stability and the kinetic inertness of the complex, both decreasing with increasing hydration number and decreasing number of coordinated ligand donors.

We have long been interested in the development of enzymatically activated imaging probes for MRI.[15–18] Our design concept involves the conjugation of an enzyme-specific substrate to a macrocyclic lanthanide chelate *via* a self-immolative spacer. The enzymatic cleavage of the substrate initiates an electronic cascade that destroys the self-immolative linker, leading to another complex, with different MRI properties (Scheme 1a). This design was later extended to multimodal detection, involving CEST and T_1 MRI, as well as optical imaging by taking advantage of the luminescent properties of lanthanide ions, emitting either in the visible or in the near-infrared range.[18] Indeed, due to their chemical similarity, different lanthanide ions can be complexed by the same ligand to provide imaging agents detectable in CEST MRI (Ln=Yb, Tb, Eu), in T_1 MRI (Ln=Gd) or in luminescence (Ln=Tb, Yb). We have first studied model complexes **LnL1** and **LnL2** where **LnL1** mimics the enzyme-specific probe, but without containing the substrate, and **LnL2** is the complex expected after enzymatic activation (Scheme 1). For these, we could demonstrate remarkable differences in relaxivity (**GdL1** vs. **GdL2**), CEST properties (**YbL1** vs. **YbL2**) as well as luminescence emission (**YbL1** vs. **YbL2**), showing the potential of these systems for the development of enzyme-activated agents for multimodal imaging detection.[18] We confirmed by luminescence lifetime measurements on the Eu analogues that the hydration state in solution changes from $q=0$ for the carbamate derivative **LnL1** to $q=1$ for the amine derivative **LnL2**, and this is responsible for the important relaxivity increase recorded for the corresponding Gd^{3+} complexes.

The present work focuses on further characterization of these model complexes **LnL1** and **LnL2**. While the crystal structure of **GdL1** was previously published,[18] we report here crystallographic data for the **CeL1** analogue as well as for **YbL2**. Concerning the stability and the inertness of the complexes, we had some specific objectives. First, in **LnL1** chelates we wanted to assess the contribution of a coordinating carbamate function, a donor group which is rarely present in Ln^{3+} complexes. Pyridine derivatives of DOTA, similar to **L2**, were reported for Ln^{3+} complexation,[19] however, to the best of our knowledge, no thermodynamic and kinetic data are available. Further, we wanted to compare both the stability and the inertness of the complexes as a function of the metal ion size between early (Ce), middle (Gd) and late (Yb) lanthanides. Finally, these structural and stability data were complemented by the characterization of the relaxation properties for **GdL2**.

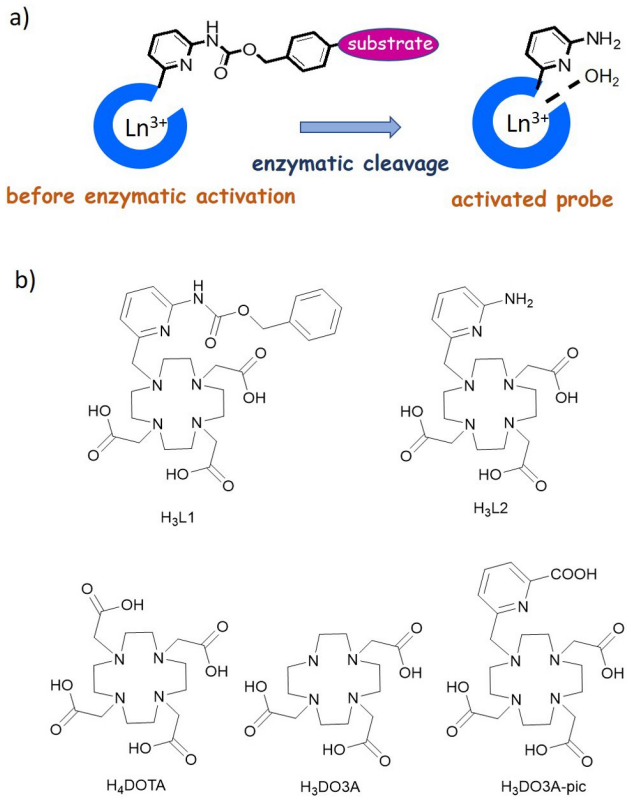

Scheme 1. a) Schematic representation of enzymatically activated, self-immolative imaging agents. b) Formulae of the ligands studied or discussed.

Results and Discussion

X-ray crystal structures

X-ray structures have been determined for **CeL1** and **YbL2** complexes. Crystals suitable for structure determination were obtained through vapor diffusion of acetone into aqueous solutions. Plots of the solid-state structures are shown in Figure 1, and selected structural data are listed in Tables 1 and 2; full crystallographic details are given in the Supporting Information. Lanthanide complexes of DOTA derivatives can potentially exist in either a square antiprismatic (SAP) or a twisted SAP (TSAP) geometry, depending on the conformation of the five-membered N–C–C–N chelate rings and the helicity of the side arms.[20] In some complexes, an eight-coordinated square antiprismatic structure without coordinated water above the O4-plane can be observed (SAP′ or TSAP′ forms).[21] The crystal structures of **CeL1** and **YbL2** exhibit high similarities, with only minor variations. Only one enantiomer of the TSAP

Research Article
doi.org/10.1002/ejic.202300784

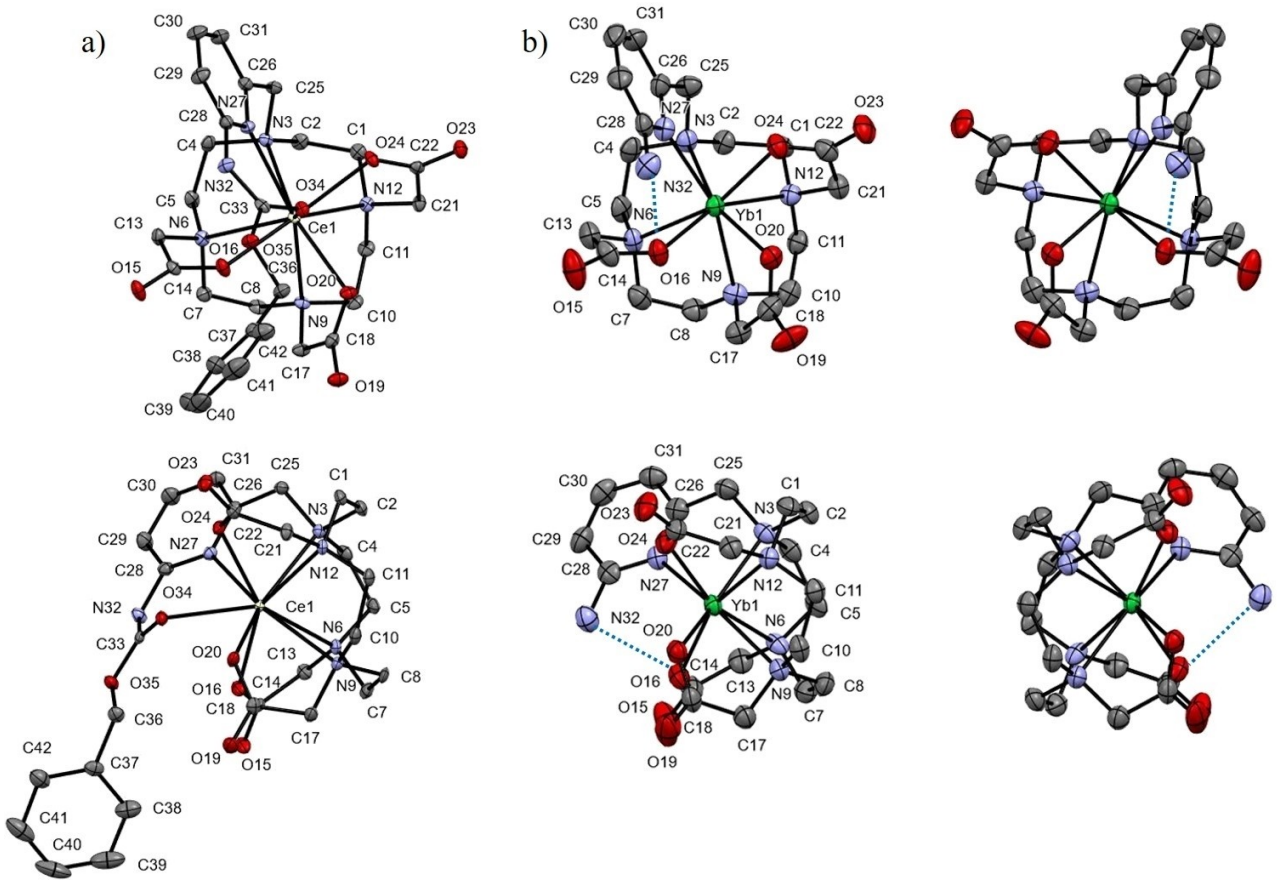

Figure 1. ORTEP-III plot[24] of a) the TSAP enantiomer Δ(δδδδ) in the unit cell of **CeL1**, b) the TSAP' enantiomers Δ(δδδδ) (left) and Λ(λλλλ) (right) in the unit cell of **YbL2** (generated from CIF using mercury software[25]). Ellipsoids are drawn at the 40% probability level, and H atoms are not shown for clarity. The macrocycle is depicted behind the lanthanide and carboxymethyl arms (top) or on the side (bottom). Intramolecular hydrogen bonds are presented as a blue dashed line.

Table 1. Bond distances in the metal coordination sphere.

	GdL1[a,b]	CeL1[c]	YbL2[d]
d(Ln–N3) (Å)	2.618(3)	2.708(3)	2.484(5)
d(Ln–N6) (Å)	2.623(3)	2.773(3)	2.568(5)
d(Ln–N9) (Å)	2.648(3)	2.695(3)	2.542(6)
d(Ln–N12) (Å)	2.663(3)	2.715(3)	2.533(5)
d(Ln–27) (Å)	2.616(3)	2.755(3)	2.519(6)
d(Ln–O16) (Å)	2.401(2)	2.433(2)	2.247(4)
d(Ln–O20) (Å)	2.321(3)	2.444(3)	2.242(4)
d(Ln–O24) (Å)	2.369(3)	2.463(3)	2.265(4)
d(Ln–O34) (Å)	2.429(3)	2.477(2)	
d(Ln–Q_{N4})[e] (Å)	1.606	1.730	1.493
d(Ln–Q_{O3N})[e] (Å)	0.779	0.866	1.077

[a] ref [7d]. [b] determined for the Δ(λλλλ) enantiomer (see supporting information). [c] determined for the Δ(δδδδ) enantiomer (see supporting information). [d] determined for the Λ(λλλλ) enantiomer (see supporting information). [e] centroids of N4-planes (PN4). [e] centroids of O3 N-planes (PO3 N).

Table 2. Geometrical parameters involving the M(III)-carbamate or amine environment.

Head 1[b]	GdL1[a,b]	CeL1[c]	YbL2[d]
d(Ln 034) (Å)	2.429(3)	2.477(2)	
d(Ln–N32) (Å)	3.698(3)	3.827(3)	3.683(6)
Λ(O20–Ln–N27) (Å)	139.56(10)	137.45(8)	122.89(17)
Λ(O16–Ln–O24) (Å)	145.77(9)	142.93(11)	126.64(17)
isomer	SA (racemic)	TSA (homochiral)	TSA' (racemic)

[a] ref. [18]. [b] determined for the Δ(λλλλ) enantiomer (see supporting information). [c] determined for the Δ(δδδδ) enantiomer (see supporting information). [d] determined for the Λ(λλλλ) enantiomer (see supporting information).

form was found in the unit cell of **CeL1** with configuration Δ(δδδδ), whereas both enantiomers of the TSAP' form were found for **YbL2** with configurations Λ(λλλλ) and Δ(δδδδ) (Figure 1). The previously reported crystal structure of **GdL1**[18] exhibited both enantiomers of the SAP form with configurations Λ(δδδδ) and Δ(λλλλ) (Figure S3). Complex geometries similar to that of **LnL1** (Ln: Ce, Gd) were reported for DOTA complexes formed with Ce^{3+} and Gd^{3+}.[21–22] On the other hand, **YbDOTA** crystallized in SAP configuration, in contrast to the TSAP' form

Research Article
doi.org/10.1002/ejic.202300784

found for **YbL2**. This difference can likely be attributed to the presence of the pyridine arm, since similar TSAP configuration was already reported for another pyridine-derived complex.[19] In **CeL1** and **YbL2**, the ligands are coordinated to the central metal ion in a nona- and an octadentate fashion, respectively. The four nitrogen atoms of the tetraazacyclododecane ring (N3, N6, N9, N12), and the pyridine nitrogen (N27) together with the three carboxylate oxygen atoms (O16, O20, O24) constitute two series of donor atoms which form square planes (N4 and O3 N planes) that are nearly parallel (angle: 2.66° and 4.51° for **CeL1** and **YbL2**, respectively). The twist angle ϕ between these two square planes is 21.75° and 24.22° for **CeL1** and **YbL2**, respectively (see supporting information), typical of TSAP/TSAP' geometry.[21] The Ce^{3+} ion of **CeL1** is slightly farther from the O3 N plane (0.866 Å) and closer to the N4 plane (1.730 Å) than in **CeDOTA** (0.7677 Å and 1.7628 Å, respectively).[21] **YbL2** has a similar behavior in comparison to **YbDOTA** (1.077 Å vs 0.728 Å and 1.493 Å vs 1.588 Å).[21] These differences can also be related to the preference of Ln^{3+} ions for carboxylate O over pyridine N donors, as confirmed by the longer distance of Ln–N(Pyridine) than Ln–O(carboxylate) in both **CeL1** and **YbL2** (see d(Ln–N27) and d(Ln–Ox), Table 1).

In **CeL1**, the Ln^{3+} ion is nine-coordinate, as the square antiprism is capped by the oxygen atom of the carbamate (O34), like in **GdL1**,[18] while no capping ligand is present in **YbL2**. The octacoordination of the metal ion in **YbL2** is consistent with the O–Ln–O/N angles, ω ω′ of 122.64 and 122.89°, determined between *trans* annular oxygen and nitrogen atoms in the O3 N plane, known as opening angles (Table S5, Figure S4), which are lower than the proposed limiting value ≈135° for complexes with water coordination in the capping position.[23] Interestingly, the distance between the coordinated carbamate oxygen (O34) and Ce^{3+} (d(Ln–O34) = 2.429(3) Å) in **CeL1** is considerably shorter than the Ce^{3+}-water oxygen distance in **CeDOTA** (2.59(1) Å),[21] which is certainly the consequence of the covalent link between the carbamate and the pyridine in **CeL1**. Finally, an intramolecular hydrogen bond between one of the amine protons (NH32) and the coordinated oxygen atom of a proximal carboxylate (O16) is observed in both enantiomers of **YbL2**. The other amine proton is involved in an intermolecular hydrogen bond with a carboxylate of another complex (O23) with the same chirality (Table S3 and Figure S2). The intramolecular hydrogen bond can contribute to the stabilization of the complex and affect the protonation constant of the amine. For **CeL1**, we observed only intermolecular hydrogen bonds between the carbamate proton (NH32) and the carboxylate (O15) of another complex, and between all carboxylate oxygens and the network of surrounding water molecules (Table S2 and Figure S2a).

Protonation constants of the ligands and stability constants of the complexes

Protonation constants, $\log K_{Hi}$, of the ligands **L1** and **L2** have been determined by pH-potentiometric titrations at 0.15 M NaCl ionic strength. They are shown in Table 3, together with

Table 3. Ligand protonation constants ($I = 0.15$ M NaCl, 25 °C).

	L1	L2	DOTA[a]	DO3A[b]	DO3A-pic[c]
$\log K_{H1}$	8.97(4)	9.12(4)	9.37	10.07	9.21
$\log K_{H2}$	9.24(1)	9.29(2)	9.14	8.93	8.94
$\log K_{H3}$	4.62(3)	7.71(3)	4.63	4.43	4.82
$\log K_{H4}$	3.20(3)	4.26(4)	3.91	4.11	3.52
$\log K_{H5}$	–	2.11(3)	–	1.88	1.39
$\Sigma \log K_{Hi}$	26.03	32.49	27.05	29.42	27.88

[a] 0.1 M NaCl, ref. [30]. [b] ref. [31]. [c] ref. [32].

protonation constants for some similar tetraazamacrocyclic chelators. For all these ligands, the first two constants correspond to the protonation of two macrocyclic amine nitrogens in *trans* position. In the case of **L1** and **L2**, the first protonation constant is lower than that for DOTA or DO3A (1,4,7,10-tetraazacyclododecane-1,4,7-triacetate), analogously to what is observed for DO3A-pic (1,4,7,10-tetraazacyclododecane-1-picolinate-4,7,10-triacetate, Scheme 1). This reduced basicity of the macrocyclic amine can be related to the electron-withdrawing effect of the 2-methyl-6-pyridine-carbamate or 2-methyl-6-pyridine-amine moieties. The decrease of the amine protonation constant has also been reported upon replacement of acetate groups with 2-methyl-6-pyridine carboxylate functions in nitrilo-triacetate (NTA)[26] or in EDTA.[27]

For both **L1** and **L2**, the calculated value is slightly lower for the first than for the second protonation constant. This indicates that the two constants are very close, and in reality, they cannot be separated from each other. In this situation, it would be more rigorous to present a cumulative constant for these first two protonation steps ($\log\beta_{H1-2} = \log K_{H1} + \log K_{H2}$); nevertheless, we prefer to show the individual values in order to demonstrate that both steps occur around pH 9–9.2.

We should also note that the first protonation constants for these types of ligands are always considerably diminished at NaCl ionic background as compared to KCl or tetramethylammonium chloride solutions. Indeed, their complex formation with Na^+ is not negligible at such high (0.15 M) Na^+ concentration, as it was demonstrated previously for DOTA and DOTA derivatives, with typical stability constants between $\log K_{NaL} = 2.5–4.5$.[28–29] However, since our complexes are designed for potential *in vivo* applications, it seems more reasonable to work at a Na^+ concentration which mimics biological conditions.

The two lowest protonation constants for both **L1** and **L2** correspond to the protonation of the carboxylates. **L2** possesses an additional protonation step with $\log K_{H3} = 7.71$ which occurs on the amine function of the 6-amino-2-methylpyridine arm, leading to a considerably higher total basicity ($\Sigma \log K_{Hi}$) with respect to **L1**.

Potentiometry has been also applied to determine stability and protonation constants for complexes formed by **L1** and **L2** with lanthanide ions from the beginning (Ce^{3+}), the middle (Gd^{3+}) and the end (Yb^{3+}) of the series, as well as with the endogenous metal ions Mg^{2+}, Ca^{2+}, Zn^{2+} and Cu^{2+}. Given the

Research Article
doi.org/10.1002/ejic.202300784

slow formation of the lanthanide complexes in the pH region 2–4 where complex formation is not complete, batch samples have been used for these, with equilibration times of 3–4 weeks for **LnL2** and up to 6 months for **LnL1** samples. Direct titration was possible for the complexes of divalent metal ions. In the case of Cu^{2+}, the potentiometric titration has been supplemented with a UV-Vis study (Figure 2), since complex formation occurs at relatively low pH where electrode readings are less reliable and the pH effect of complex formation is small. The stability constants calculated are shown in Table 4.

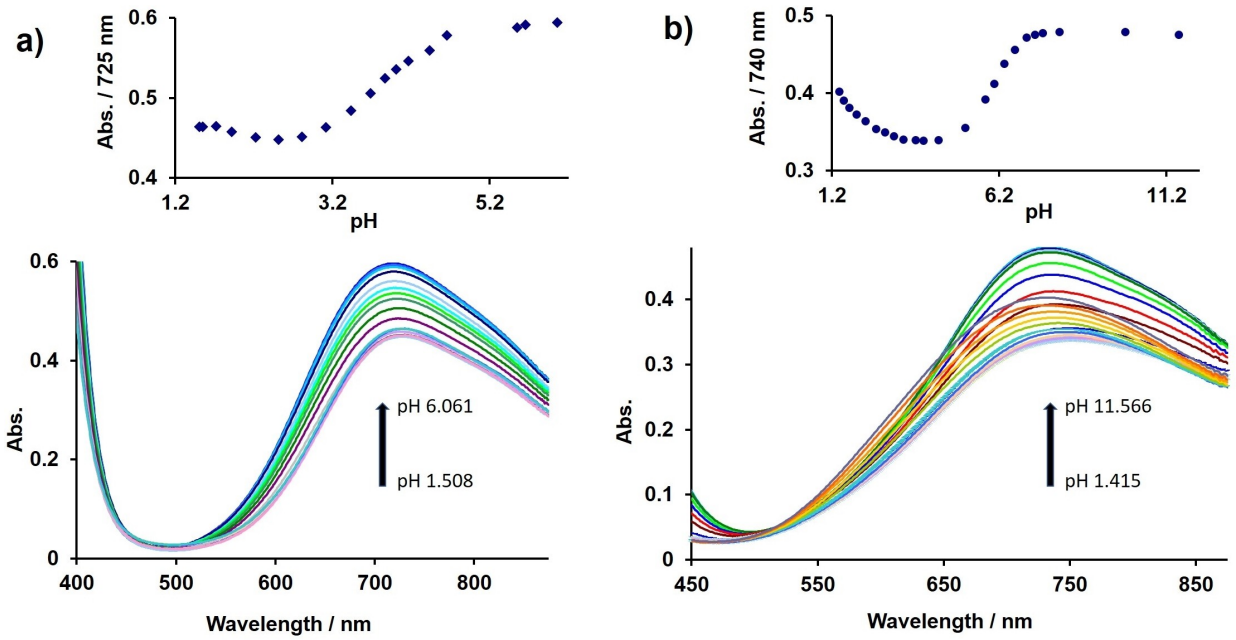

Figure 2. Variable-pH UV-Vis spectra of a) **CuL1** (1.76 mM) and b) **CuL2** (1.82 mM). The inserted figures show the variation of the absorbance at a) 725 nm and b) 740 nm, 25 °C, 0.15 M NaCl.

Table 4. Thermodynamic stability constants of ML complexes. $I = 0.15$ M NaCl, 25 °C.

		L1	L2	DO3A[a]	DOTA	DO3A-pic
Mg^{2+}	$\log K_{ML}$	7.85(1)	7.53(1)	11.64[b]	11.49[a,b]	10.44[a,g]
	$\log K_{HML}$		6.87(2)			6.89
						6.37
Ca^{2+}	$\log K_{ML}$	11.77(1)	11.88(1)	12.57[b]	16.11[a,b]	14.82[a,g]
	$\log K_{HML}$	4.16(2)	5.38(4)	4.60		4.59
						4.32
Zn^{2+}	$\log K_{ML}$	16.86(2)	16.71(5)	21.57[b]	20.21[a,b]	20.25[a,g]
	$\log K_{HML}$	3.87(2)	6.61(3)	3.47	–	4.42
	$\log K_{H2ML}$	2.93(2)	3.98(2)	2.07	–	3.06
	$\log K_{H3ML}$	–	2.96(3)	–	–	1.98
Cu^{2+}	$\log K_{ML}$	20.25(6) [c]	20.89(9)[c]	25.75[b]	24.83[a,b]	23.20[a,g]
	$\log K_{HML}$	3.89(3)	6.17(7)	3.65	–	4.17
	$\log K_{H2ML}$	3.14(1)	3.42(6)	1.69	–	3.31
	$\log K_{H3ML}$	–	2.80(4)	–	–	1.97
	$\log K_{M2L}$	3,68(4)	5,09(13)	–	–	–
	$\log K_{HM2L}$	–	5.46(6)	–	–	–
	$\log K_{H-1M2L}$	–	7.81(26)	–	–	–
Ce^{3+}	$\log K_{ML}$	18.74(4)	16.7(2)	19.7	23.4[d,e]	–
	$\log K_{HML}$		4.1(1)			
Gd^{3+}	$\log K_{ML}$	20.16(4)	18.60(6)	21.56	24.7[d,f]	23.31[h]
	$\log K_{HML}$		3.92(5)			2.65
Yb^{3+}	$\log K_{ML}$	21.1(1)	18.16(6)	–	25.0[d,e]	–
	$\log K_{HML}$		4.17(5)			
pGd		17.7	15.5	15.8	19.2	20.96

[a] $I = 0.1$ M KCl. [b] ref. [33] [c] data obtained from combined analysis of potentiometric and UV-Vis data, [d] 0.1 M NaCl; [e] ref. [36–37]; [f] ref. [30]; [g] ref. [34]; [h] ref. [32].

Research Article
doi.org/10.1002/ejic.202300784

With divalent metal ions, ligands **L1** and **L2** form complexes of similar stability, despite their different denticity. This is expected since with a typical coordination number of six, these small M^{2+} cations cannot accommodate the additional carbamate donor group of **L1**. A similar phenomenon has been observed for instance in the case of the Cu^{2+} complex of **DO3A-SA** (DO3A-arylsulphonamide)[33] or the Ca^{2+}, Mg^{2+}, Cu^{2+}, Zn^{2+}, Cd^{2+} and Pb^{2+} complexes of **DO3A-pic**.[34] With Cu^{2+}, we have detected the formation of dinuclear $\mathbf{Cu_2L}$ complexes of relatively high stability ($\log K_{Cu2L} \approx 3.5–5.1$), which allowed us to titrate the samples in the presence of Cu^{2+} excess up to pH = 6.5 and 9.0 for **L1** and **L2**, respectively, without any precipitation. We also attempted to analyze the titration data for Zn^{2+} by including dinuclear complexes. However, very low stability constants of $\log K_{Zn2L} \approx 1.4$ were obtained with significant errors (st. dev. >0.3), thus dinuclear complexes were not included in the final equilibrium model.

In contrast to the divalent metals, lanthanides form more stable complexes with **L1** than with **L2**. The coordination number of Ln^{3+} ions is typically eight or nine, thus all nine donor atoms of **L1** can bind to the metal ion, leading to higher stability than the octadentate **L2**. Indeed, coordination of the carbamate function to the Ln^{3+} ion in **LnL1** complexes has been evidenced by X-ray crystal structures for **GdL1**[18] and **CeL1**. For both ligands, we observe the same stability trend along the lanthanide series, which has also been commonly reported for polyamino-polycarboxylate chelates, i.e. an increase from the beginning to the middle of the series, followed by a relatively constant stability for the complexes of heavier elements.

The $\log K_{ML}$ stability constants are lower for the complexes formed by **L1** with respect to the reference ligands **DOTA**, **DO3A** or **DO3A-pic**. One reason is the lower overall basicity of **L1**, but one should also consider that several constants in Table 3 have been determined in KCl ionic strength, making direct comparison difficult. Indeed, the stronger complex formation with Na^+ vs. K^+ results in more important competition and consequently lower stability constants in NaCl medium.

All complexes formed with **L2** possess a protonation constant corresponding to the protonation of the amine on the pyridine ring. This amine is not coordinating to the metal ion, as shown by the X-ray structure of **YbL2**. As expected, this protonation step occurs at much lower pH in the complexes than in the ligand ($\log K_{H3} = 7.71$). This diminution of the protonation constant is strongly dependent on the metal charge: it is notably larger for the complexes of the trivalent lanthanide ions ($\log K_{HML} = 3.92–4.17$) than for those of divalent metals ($\log K_{HML} = 5.38–6.87$). Importantly, for all Ln^{3+} complexes, the amine is deprotonated at physiological pH, leading to neutral species. It is interesting to note that this pyridinic amine is more acidic than the exocyclic amine of the amino glycine arm in **Gd(DOTA-α-NH$_2$)** (Scheme 1) ($\log K_{HML} = 5.12$)[17]. We note that the stability constant determined for **GdL2** is about 5 orders of magnitude lower than what could be estimated based on empirical equations derived from a large database,[35] likely related to the limited examples available on pyridine-derivatives.

In order to overcome the problems of different conditions used and of different ligand basicities when comparing the stabilities, we have calculated the pGd values ($pGd = -\log[Gd]_{free}$ at $c_{Gd} = 10^{-6}$ M, $c_{lig} = 10^{-5}$ M, pH 7.4; Table 4). These data unambiguously show the superior stability of the complexes formed with the higher-denticity carbamate vs. the amine derivative. When comparing the two nonadentate ligands **L1** and **DO3A-pic**, the much higher pGd value found for **Gd(DO3A-pic)** evidences the stronger metal coordination of the negatively charged carboxylate donor with respect to the non-charged carbamate on the pyridine pendant. In addition to this charge effect, the chelate ring size (5-membered for the picolinate and 6-membered for the 6-pyridinyl-carbamate) further contributes to the stability difference. In overall, we can conclude that both **L1** and **L2** form lanthanide complexes of sufficiently high stability for potential *in vivo* use.

Dissociation kinetics of the lanthanide complexes

In addition to good thermodynamic stability, the kinetic inertness of the lanthanide complexes also needs to be sufficiently high to avoid the release of free, toxic metal ions. Thanks to the rigid and pre-organized structure of macrocyclic DOTA-type chelators, in their complexes, the coordination sphere of the lanthanide ion is not accessible for the competitor ligands. Further, the metal coordination of the carboxylate pending arms yields compact structures which, in the absence of potential coordinating sites for competitor metal ions, prevents the formation of dinuclear complexes. The latter could induce metal-catalyzed dissociation. In overall, this leads to very slow dissociation, occurring exclusively *via* proton-assisted pathways.

Therefore, in order to characterize the inertness of **GdL1** and **LnL2** (Ln=Ce, Gd, Yb) complexes, we have first followed their dissociation in highly acidic conditions (0.05 M – 0.3 M HCl for **LnL2** and 0.01–1.2 M HCl for **GdL1**). Under these conditions, the complexes are not stable and dissociate completely. Given the very high H^+ concentration, the dissociation follows a pseudo-first order kinetics and the dissociation rate is directly proportional to the total concentration of the complex $[\mathbf{LnL}]_t$ (corresponding to the sum of the concentration of protonated and non-protonated complexes), where k_{obs} is the observed pseudo-first order rate constant:

$$-\frac{d[\mathbf{LnL}]_t}{dt} = k_{obs}[\mathbf{LnL}]_t \quad (1)$$

The dissociation reactions have been followed by monitoring the increase in the longitudinal proton relaxation rate in the case of **GdL1** (1 mM), or by UV-Vis spectrophotometry by monitoring the decrease of the absorbance of the complexes at 350 nm in the case of the three **LnL2** complexes ($c \approx 0.25$ mM). The dependence of the observed pseudo-first order dissociation rate constants on the proton concentration is shown in Figure 3.

Research Article
doi.org/10.1002/ejic.202300784

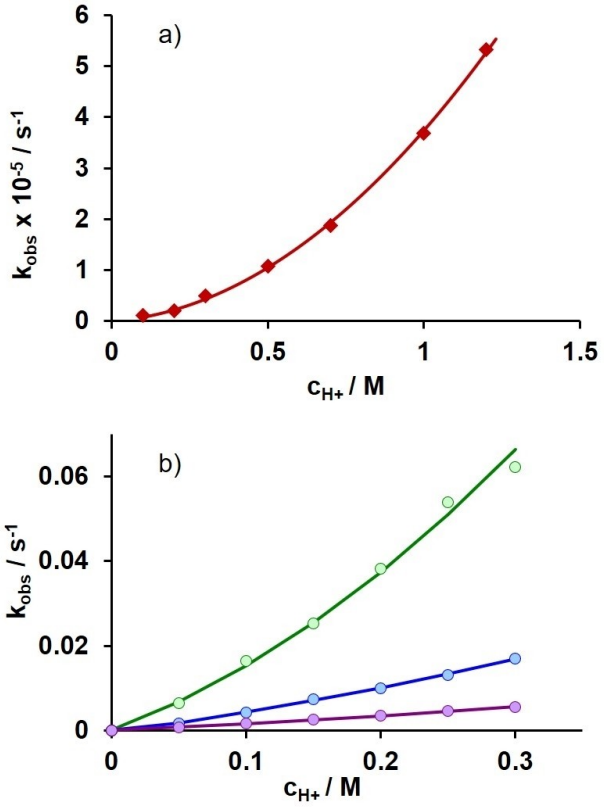

Figure 3. Dependence of the pseudo-first order dissociation rate constants on the acid concentration in highly acidic conditions for a) **GdL1** and b) **CeL2** (●; 0.225 mM; **GdL2** (●; 0.247 mM) and **YbL2** (●; 0.251 mM) complexes; 25 °C; $I = 1$ M NaCl. The lines correspond to the fit of the experimental data.

For all **LnL1** and **LnL2** complexes, the k_{obs} values show a second order dependence on [H^+], as it has often been observed for both macrocyclic and acyclic lanthanide chelates. This indicates that Gd^{3+} release might occur *via* spontaneous dissociation or by acid-catalyzed dissociation of the non-protonated or of the protonated complexes, characterized by rate constants k_0, k_1 and k_2, respectively:

$$k_{obs} = k_0 + k_1[H^+] + k_2[H^+]^2 \quad (2)$$

The k_{obs} data in Figure 3 have been fitted to eq. 2 to obtain the individual rate constants. In all cases, very small, sometimes negative, values have been calculated for k_0, with large errors, which led us to fix k_0 to zero and calculate only k_1 and k_2. This indicates that the spontaneous pathway does not contribute to the dissociation under our conditions. The calculated rate constants are presented in Table 5, together with the dissociation half-lives extrapolated to pH 7.4.

When comparing the data in Table 5, we can draw several conclusions. First of all, we note the extremely high inertness of **GdL1**, with a similar k_1 value to that of **GdDOTA**. Their estimated dissociation half-lives, $t_{1/2}$, are very different, because at physiological pH, the spontaneous dissociation is an important contributor for **GdDOTA**; however, this could not be assessed under our conditions for **GdL1**, therefore it seems more reasonable to compare the k_1 values.

The inertness is considerably decreased for the complexes of amine derivative, with 4-orders of magnitude higher k_1 values, similar to that reported for the seven-coordinate **GdDO3A**. The low inertness of the **LnL2** complexes is linked to the lower denticity of the ligand with respect to **L1**, but even more importantly, to the presence of the protonation site (non-coordinated amine) which largely accelerates the proton-assisted dissociation. The protonation of the amine can potentially induce the decoordination of the pyridine as well. It has previously been demonstrated that for these polyazamacrocyclic complexes, the rate-determining step of the dissociation is the proton transfer to the macrocyclic nitrogen which then leads to the release of the metal ion.[39] This process is easier for **GdL2**, with an amine possessing a relatively high protonation constant ($\log K_{HGdL} = 3.92$), than for **GdL1** which can be protonated exclusively on a carboxylate function and only at low pH (the protonation constant could not even be determined by potentiometry). Similar observations have been made for other chelates containing protonable groups, such as phosphonates.[40–41]

Table 5. Rate constants characterizing the dissociation of **LnL** complexes, determined at 0.01–1.2 M HCl or from transmetallation experiments with Cu^{2+}. 25 °C.

	k_0 (s^{-1})	k_1 ($M^{-1}s^{-1}$)	k_2 ($M^{-2}s^{-1}$)	$t_{1/2}$ (h)
GdL1	0[a]	$(6.38 \pm 0.01)\times10^{-6}$	$(3.0 \pm 0.3)\times10^{-5}$	7.6×10^{8}
CeL2	0[a]	$(1.18 \pm 0.09)\times10^{-1}$ $(2.1 \pm 0.1)\times10^{-2}$ [d]	$(3.4 \pm 0.5)\times10^{-1}$	4.1×10^{4} 2.2×10^{5} [d]
GdL2	0[a]	$(4.5 \pm 0.2)\times10^{-2}$ $(1.6 \pm 0.2)\times10^{-3}$ [d]	$(4.6 \pm 0.7)\times10^{-2}$	1.1×10^{5} 3.2×10^{6} [d]
YbL2	0[a]	$(1.46 \pm 0.03)\times10^{-2}$	$(1.4 \pm 0.2)\times10^{-2}$	3.3×10^{5}
GdDO3A[b]	0[a]	2.3×10^{-2}	–	2.1×10^{5}
GdDOTA[c]	6.7×10^{-11}	1.8×10^{-6}	–	2.9×10^{6}
EuDO3A-pic		1.56×10^{-3}		3.1×10^{6}

[a] fixed during the fitting procedure; [b] 0.1 M KCl, 25 °C ref. [33]; [c] 0.15 M NaCl, 25 °C ref. [38]; [d] from Cu-transmetallation experiments, pH 3.1–4.7.

Research Article
doi.org/10.1002/ejic.202300784

The comparison of **CeL2**, **GdL2** and **YbL2** complexes underlines the importance of the lanthanide ion size for kinetic inertness. Indeed, there is continuous decrease in k_1 from **CeL2** to **GdL2** and to **YbL2**, which corresponds to a tenfold enhancement of the inertness from the beginning to the end of the lanthanide series. Given the importance of the proton-assisted processes for the dissociation, one can explain this trend by the increasing repulsion of the proton by the smaller lanthanides which are characterized by higher charge density.

In order to better approach physiological conditions, we have also studied dissociation of **CeL2** and **GdL2** in the pH range 3.1–4.7, and in the presence of Cu^{2+} excess (Figure 4). The reaction was monitored by UV-Vis spectrophotometry for **CeL2** and by relaxometry for **GdL2**. Dissociation is very slow under these conditions, thus the reactions had to be followed for several months.

In this pH range, the k_{obs} data show a linear dependence on H^+ concentration, therefore the determination of k_2 values is not possible. Unfortunately, it was also impossible to obtain reliable data for k_0, as the fit yielded negative values with large errors for both complexes. For k_1, about one order of magnitude lower constants have been obtained from the fit for both **CeL2** and **GdL2**, as compared to those determined from the high acidity data (see above, Figure 3 and Table 3), implying a tenfold increase in the dissociation half-lives that can be estimated for pH 7.4.

These findings clearly demonstrate the difficulties to determine reliable dissociation kinetic constants for the characterization of highly inert complexes. While the measurements are easier (faster) under very acidic solutions, these are far from the physiological conditions and the extrapolation to pH 7.4 is uncertain. On the other hand, at pH values closer to 7.4, the very slow dissociation requires extremely long periods for the monitoring with all the experimental difficulties associated. Independently of this issue, we can conclude that all these complexes, and particularly **LnL1**, are endowed with excellent resistance to dissociation.

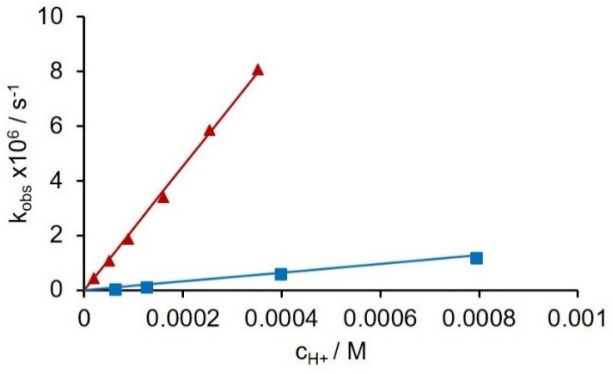

Figure 4. Dependence of the pseudo-first order dissociation rate constants on the acid concentration in Cu-transmetallation experiments for **CeL2** (▲) and **GdL2** (■). **CeL2**: pH 3.45–4.73, cCeL2 = 0.15 mM, c_{Cu2+} = 4.5 mM; **GdL2**: pH 3.1–4.2, c_{GdL2} = 1 mM, c_{Cu2+} = 10 mM 25 °C; I = 0.15 M NaCl.

^{17}O NMR and NMRD measurements on GdL2

The ^{17}O and ^{1}H relaxation properties have been investigated for **GdL2** which contains one inner sphere water molecule, as previously determined by luminescence lifetime measurements on the Eu^{3+} analogue.[18] The MRI efficiency of paramagnetic metal complexes is expressed by their proton relaxivity, r_1, which is defined as the paramagnetic enhancement of the longitudinal relaxation rate induced by 1 mM concentration of the complex. The proton relaxivity of **GdL2** has been measured in the range of 0.04–128 MHz proton Larmor frequency, at 25 °C and 37 °C (Figure 5). The shape of these Nuclear Magnetic Relaxation Dispersion (NMRD) profiles and the relaxivity values are in accordance with a monohydrated, small molecular weight Gd^{3+} chelate. These data have been complemented by the measurement of variable temperature ^{17}O transverse relaxation rates and chemical shifts at 9.4 T (Figure 5), which give direct access to the water exchange rate. For **GdL1**, the relaxivities were previously reported and they are much lower, as expected for a non-hydrated chelate.[18]

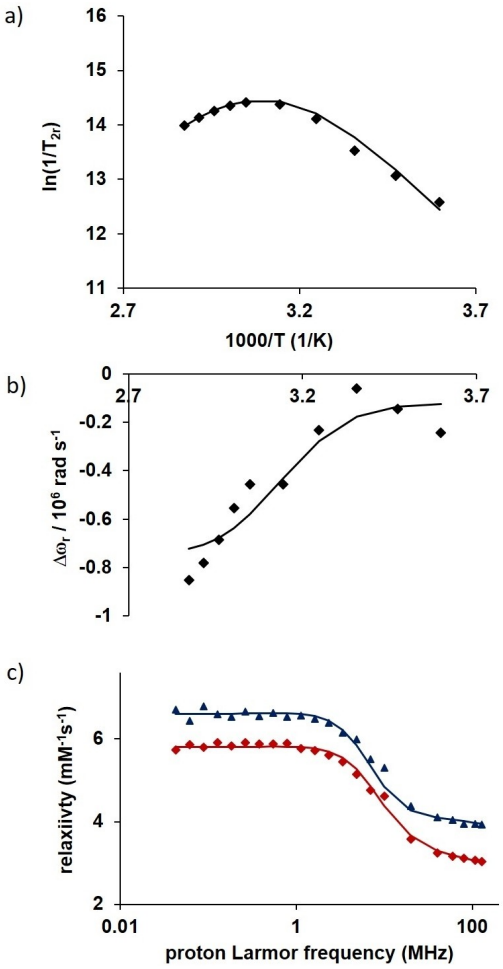

Figure 5. 17O transverse relaxation rates (a), ^{17}O chemical shifts (b) (9.4 T, c_{GdL2} = 17.7 mmol/kg), and NMRD profiles (1.79 mM) at 25 °C (▲) and 37 °C (♦) (c) measured for **GdL2**. The solid lines represent the simultaneous fit to all data as explained in the text.

Research Article
doi.org/10.1002/ejic.202300784

The ^{1}H NMRD and the ^{17}O NMR data have been analyzed together according to the Solomon-Bloembergen-Morgan theory of paramagnetic nuclear relaxation.[42] We have calculated the rate (k_{ex}^{298}), the enthalpy ($\Delta H^{\neq}$) and the entropy ($\Delta S^{\neq}$) of the water exchange, the rotational correlation time (τ_R^{298}), its activation energy (E_R), the ^{17}O scalar coupling constant ($A/\hbar$), and the parameters characterizing electron spin relaxation (τ_v^{298} and Δ^2). Some parameters were fixed in the fit to common values, such as the activation energy for the modulation of the zero-field splitting to $E_v = 1$kJ/mol, the Gd–H distance to 3.1 Å, and the diffusion constant to $D_{GdH}^{298} = 26$ kJ/mol. The calculated parameters are listed in Table 6 and compared to those for **GdDOTA**. The list of all equations used in the analysis can be found in the supporting information.

Most of the parameters have similar values for **GdL2** and for the tetraacetate derivative **GdDOTA**, except for the water exchange rate which is decreased by a factor of three for **GdL2**. At the same time, the highly positive activation entropy indicates a strong dissociatively activated water exchange process, implying that the departure of the coordinated water molecule is the rate-determining step. In such processes, the charge of the complex has an important role: in a complex with a less negative charge, such as **GdL2**, the leaving water molecule will experience a stronger electrostatic attractive force from the positively charged metal center. This makes the dissociative step energetically less favored, leading to a slower water exchange. Moreover, the Gd–N(pyridine) distance can be also expected considerably longer than the distance between the Gd and carboxylate oxygens in **GdDOTA**, resulting in less steric constraint around the coordinated water. This also leads to slower water exchange in the case of dissociative activation, as it was previously demonstrated in several cases.[43–44] In overall, we can conclude that the substitution of one negatively charged, small acetate function of **GdDOTA** with a neutral pyridine in **GdL2**, implying a longer Gd–N bond distance, results in a less efficient water exchange. Nevertheless, this decrease in the water exchange rate does not have negative consequences on the proton relaxivity of **GdL2**, which remains exclusively limited by fast rotation.

The rotational correlation time, τ_R^{298}, has a value which corresponds to the size of the complex. We note that the scalar coupling constant has a negative sign in the formalism of the Solomon-Bloembergen-Morgan equations used (supporting information), although it should be theoretically positive as the consequence of a negative spin density at the oxygen nucleus and the negative magnetic moment of the ^{17}O nucleus, as it was demonstrated by different authors.[45–46] The electron spin relaxation is notably faster for **GdL2** than for **GdDOTA**, as expressed by its seven times higher Δ^2 value (Table 6). This is likely related to the lower symmetry of **GdL2** which is known to affect electron spin relaxation.[47]

Table 6. Parameters calculated from the fit of ^{17}O NMR and NMRD data.

	GdL2	GdDOTA[a]
k_{ex}^{298} / 10^6 s^{-1}	1.3 ± 0.1	4.1
$\Delta H^{\neq}$ / kJ mol^{-1}	52.4 ± 2.6	49.8
$\Delta S^{\neq}$ / J mol^{-1}K^{-1}	+48 ± 5	+48.5
E_R / kJ mol^{-1}	27.6 ± 0.6	16.1
τ_R^{298} / ps	76 ± 3	77
τ_v^{298} / ps	12 ± 1	11
Δ^2 / 10^{20} s^{-2}	1.1 ± 0.1	0.16
$A/\hbar$ / 10^6 rad s^{-1}	−3.4 ± 0.2	−3.7

[a] ref. [48].

Conclusions

In the general context of contrast agent design for the detection of enzymatic activities, two tetraazamacrocyclic ligands bearing three carboxylates and an additional pyridine-carbamate (**L1**) or pyridine-amine (**L2**) pendant arm have been investigated for their lanthanide complexation properties. Solid-state structures have been evaluated by X-ray crystallography for **CeL1** and **YbL2** and demonstrated nine- and eight-coordinate complexes, respectively, without inner sphere coordinated water. Thermodynamic stability constants have been determined for complexes of **L1** and **L2** formed with different lanthanides and divalent metal ions. Lanthanides form more stable complexes with **L1** than with **L2** due to the higher denticity of the ligand with carbamate, while there is no difference in stability between **ML1** and **ML2** complexes for the smaller metals Mg^{2+}, Ca^{2+}, Zn^{2+} or Cu^{2+}. **GdL1** has a remarkably high kinetic inertness, while **GdL2** dissociates faster, due to an acceleration of proton-assisted dissociation induced by the presence of the protonable amine function. Finally, the ^{1}H and ^{17}O relaxation properties have been also assessed for the monohydrated **GdL2** chelate. Most importantly, its water exchange was found to be three times slower than that of **GdDOTA**, related to the decreased negative charge of the pyridine and the longer Gd–N(pyridine) distance, both leading to a disfavored departure of the leaving water molecule in a dissociatively activated water exchange process. In overall, we can conclude that the lanthanide complexes of both **L1** and **L2** ligands are sufficiently stable and inert for the development of molecular imaging agents.

Experimental Section

Ligands **L1** and **L2**, as well as the **LnL1** and **LnL2** complexes have been synthesized and characterized according to previously reported procedures.[18]

X-ray crystal structures

Crystallographic data (see details in the SI -XR analysis) for the structures of **CeL1** and **YbL2** have been deposited with the Cambridge Crystallographic Data Centre, CCDC, 12 Union Road, Cambridge CB21EZ, UK. Copies of the data can be obtained free of charge on quoting the depository numbers CCDC 2299208 (**CeL1**) and 2299209 (**YbL2**), respectively (Fax: +44-1223-336-033; mail: deposit@ccdc.cam.ac.uk, http://www.ccdc.cam.ac.uk).

Protonation and stability constant determination

Potentiometric titrations were performed in order to determine protonation constants (defined by Eq. 3) for the ligands **L1** and **L2** and stability and protonation constants (Eqs. 4–8) of the complexes formed with Zn^{2+}, Cu^{2+}, Mg^{2+} and Ca^{2+} metal ions at different metal to ligand ratios (1:1 and 2:1).

$$K_{Hi} = \frac{[H_iL]}{[H_{i-1}L][H^+]} \quad i = 1 - 5 \tag{3}$$

$$K_{ML} = \frac{[ML]}{[M][L]} \tag{4}$$

$$K_{HiML} = \frac{[MH_iL]}{[MH_{i-1}L][H^+]} \tag{5}$$

$$K_{M2L} = \frac{[M_2L]}{[ML][M]} \tag{6}$$

$$K^{H}_{M2L} = \frac{[M_2HL]}{[M_2L][H^+]} \tag{7}$$

$$K^{H^{-1}}_{M2L} = \frac{[M_2H^{-1}L][H^+]}{[M_2L]} \tag{8}$$

Titrations were carried out with a Metrohm 888 Titrando automatic titration system and with a Metrohm combined electrode in a cell thermostated at 25 °C. All titrations were performed at 0.15 M NaCl ionic strength, by adding ~0.2 M NaOH solution to a ~2 mM solution of the ligand, in 6 mL total volume. The cell content was stirred by using a magnetic stirrer and N_2 (g) was bubbled through to insure inert atmosphere. Titrations were performed between pH 1.78–11.85, or until metal hydroxide precipitation occurred (in the samples with metal excess). HCl was added to the starting solution to obtain a starting pH value of 2. H^+ ion concentrations were obtained from the measured pH values using the method of Irving et al.[49]

Owing to the relatively slow complexation between macrocyclic ligands and Ln^{3+} ions, the "out-of-cell" technique was used to determine stability and protonation constants of **LnL1** and **LnL2** complexes. Thirteen samples of 1.50 mL total volume were prepared containing known ligand and Ln^{3+} concentrations (1.95 mM **GdL1**, 1.92 mM **CeL1**, 1.95 mM **YbL1**, 1.91 mM **GdL2**, 1.88 mM **CeL2**, 1.91 mM **YbL2**). The pH of the samples was adjusted by HCl or NaOH solutions (approximately 0.2 M) to set the pH into the range where complexation is expected to take place. The samples were sealed under nitrogen gas and incubated at 25 °C until equilibrium (6–7 months for **LnL1** and 3–4 weeks for **LnL2**; the time required to reach equilibrium was estimated by using ^{1}H-relaxivity measurements in duplicate samples). Samples were then opened and pH values were measured using a pH-meter equipped with a Metrohm combined electrode. The PESQUAD program was used for the calculation of the equilibrium constants.[50]

For the determination of the stability constants of **CuL1** and **CuL2** complexes, UV-visible absorption spectra (λ = 350–875 nm, 25 °C) were recorded on a Cary 1E UV-vis spectrometer, in individual batch samples at varying pH values (pH = 1.51–6.06 for **CuL1** and pH = 1.42–11.57 for **CuL2**; c_{CuL} = ~1.80 mM, I = 0.15 M NaCl and l = 2 cm). Another series of batch samples were prepared by using considerably higher acid concentration (0.0614 to 0.762 M and 0.0624 to 0.762 M, for **CuL1** and **CuL2**, respectively) and all data obtained by pH-potentiometric titration (1:1 and 2:1 metal to ligand ratio) as well as VIS spectroscopy were fitted simultaneously with the PESQUAD program. Molar absorption of the $CuCl_2$ and that of **CuL1** and **CuL2** complexes were determined independently, while those of the protonated species were refined during the calculation.

Dissociation kinetic studies

Proton-assisted dissociation kinetics was investigated in acidic solutions for **GdL1** (0.1–1.2 M HCl; c_{GdL1} = 1 mM), **GdL2** (0.05–0.3 M HCl; c_{GdL2} = 0.247 mM), **CeL2** (0.05–0.3 M HCl; c_{CeL2} = 0.233 mM) and **YbL2** (0.05–0.3 M HCl; c_{YbL2} = 0.250 mM); at 25 °C and I = 1 M NaCl ionic strength. Under such acidic conditions, the complexes fully dissociate. The dissociation was monitored either via the relaxivity increase at 20 MHz (**GdL1**) or *via* the decrease in the UV-Vis absorbance at 305 nm (**LnL2** complexes).

Cu^{2+}-catalyzed dissociation kinetic studies were performed under pseudo-first-order conditions, using a standard UV-spectrophotometric method for **CeL2** or by following the relaxivity increase (20 MHz) for **GdL2**, under the following conditions: **CeL2**: pH 3.45–4.73, 50 mM *N*-methyl-piperazine (NMP) buffer, c_{CeL2} = 0.15 mM, c_{Cu2+} = 4.5 mM; **GdL2**: pH 3.1–4.2, 50 mM NMP, c_{GdL2} = 1 mM, c_{Cu2+} = 10 mM; I = 0.15 M NaCl; 25 °C.

Pseudo-first-order rate constants (k_{obs}) were calculated by fitting the absorbance vs. time data or the relaxivity vs. time data to the following equation:

$$X_t = (X_0 - X_e)e^{-k_{obs} \times t} + X_e \tag{9}$$

where X_t, X_0 and X_e are the absorbance or relaxivity values at time t, at the beginning and at the end of the reaction, respectively. The calculations were performed with the computer program Scientist, by using a standard least-squares procedure.

Relaxivity measurements

^{1}H NMRD profiles of aqueous **GdL2** solution (c_{GdL2} = 1.79 mM, determined by bulk magnetic susceptibility (BMS) measurements; pH = 7.1) were recorded at 25 and 37 °C on a SMARTracer Fast Field Cycling NMR relaxometer (Stelar; 0.00024–0.24 T, 0.01–10 MHz ^{1}H Larmor frequency), a WP80 NMR electromagnet adapted to variable-field measurements (Bruker; 0.47–1.88 T, 20–80 MHz ^{1}H Larmor frequency), and a Stelar High Field relaxometry system with a 3T variable field magnet 10–128 MHz). The temperature was maintained by a gas flow and monitored by a VTC91 temperature control unit, based on previous calibration with a Pt resistance temperature probe.

^{17}O NMR Measurements

Variable-temperature ^{17}O NMR measurements of aqueous solution of **GdL2** (c_{GdL2} = 17.7 mmol.kg^{-1}, determined by BMS measurements; pH = 7.1) were performed on a Bruker Avance III 400 MHz spectrometer (9.4 T, 54.2 MHz) in the temperature range 5–75 °C. The temperature was calculated after calibration with ethylene glycol and MeOH. Acidified water ($HClO_4$, pH = 3.3) was used as a diamagnetic reference. The ^{17}O transverse relaxation times (T_2) were obtained using the CPMG spin-echo technique. To eliminate susceptibility contributions to the chemical shift, the sample was in a glass sphere placed in a 10 mm NMR tube. To improve sensitivity, ^{17}O-enriched water (11.10% $H_2{}^{17}O$, Cortecnet) was added to the solution to yield approximately 1% ^{17}O enrichment.

The ^{17}O NMR and NMRD data have been treated according to the Solomon-Bloembergen-Morgan theory of paramagnetic relaxation and the Swift-Connick equations.[42] The least squares fit was performed using Visualiseur/Optimiseur running on a MATLAB 8.3.0 (R2014a) platform.

Supporting Information

The authors have cited additional references[51–61] within the Supporting Information.

Acknowledgements

The research was funded by the French National Research Agency ANR (grant ANR-2010-1513-01) and the Hungarian National Research, Development and Innovation Office (NKFIH PD-138064, K-128201 and K-134694 projects). Financial support from the Institute of Chemistry of Natural Substances (ICSN) for R. J. is greatly acknowledged.

Conflict of Interests

The authors declare no conflict of interest.

Data Availability Statement

The data that support the findings of this study are available in the supplementary material of this article.

Keywords: Lanthanide complexes · macrocyclic ligands · structure · stability · inertness

[1] A. Merbach, L. Helm, E. Toth, *The Chemistry of Contrast Agents in Medical Magnetic resonance Imaging*, Second Edition ed., John Wiley & Sons, Chichester, **2013**.
[2] J. Wahsner, E. M. Gale, A. Rodríguez-Rodríguez, P. Caravan, *Chem. Rev.* **2019**, *119*, 957–1057.
[3] H. Li, T. J. Meade, *J. Am. Chem. Soc.* **2019**, *141*, 17025–17041.
[4] D. V. Hingorani, A. S. Bernstein, M. D. Pagel, *Contrast Media Mol. Imaging* **2015**, *10*, 245–265.
[5] C. S. Bonnet, L. Tei, M. Botta, E. Toth, in *The Chemistry of Contrast Agents in Medical Magnetic Resonance Imaging*, 2nd Edition ed. (Eds.: A. E. Merbach, L. Helm, E. Toth), John Wiley & Sons, Chichester, **2013**, pp. 343–385.
[6] E. Vinogradov, A. D. Sherry, R. E. Lenkinski, *J. Magn. Reson.* **2013**, *229*, 155–172.
[7] S. Viswanathan, Z. Kovacs, K. N. Green, S. J. Ratnakar, A. D. Sherry, *Chem. Rev.* **2010**, *110*, 2960–3018.
[8] A. Rodríguez-Rodríguez, M. Zaiss, D. Esteban-Gómez, G. Angelovski, C. Platas-Iglesias, *Int. Rev. Phys. Chem.* **2021**, *40*, 51–79.
[9] Y. G. Li, V. R. Sheth, G. S. Liu, M. D. Pagel, *Contrast Media Mol. Imaging* **2011**, *6*, 219–228.
[10] D. V. Hingorani, E. A. Randtke, M. D. Pagel, *J. Am. Chem. Soc.* **2013**, *135*, 6396–6398.
[11] I. Daryaei, K. M. Jones, M. D. Pagel, *Chem. Eur. J.* **2017**, *23*, 6514–6517.
[12] R. A. Moats, S. E. Fraser, T. J. Meade, *Angew. Chem. Int. Ed.* **1997**, *36*, 726–728.
[13] A. Y. Louie, M. M. Huber, E. T. Ahrens, U. Rothbacher, R. Moats, R. E. Jacobs, S. E. Fraser, T. J. Meade, *Nat. Biotechnol.* **2000**, *18*, 321–325.
[14] E. Brucher, G. Tircso, Z. Baranyai, Z. Kovacs, A. D. Sherry, in *The Chemistry of Contrast Agents in Medical Magnetic Resonance Imaging* (Eds.: A. Merbach, L. Helm, E. Toth), Wiley & Sons Ltd, Chichester, UK, **2013**, pp. 157–208.
[15] R. Pollet, C. S. Bonnet, P. Retailleau, P. Durand, É. Tóth, *Inorg. Chem.* **2017**, *56*, 4317 − 4323.
[16] T. Chauvin, P. Durand, M. Bernier, H. Meudal, B. T. Doan, F. Noury, B. Badet, J. C. Beloeil, E. Toth, *Angew. Chem. Int. Ed.* **2008**, *47*, 4370–4372.
[17] T. Chauvin, S. Torres, R. Rosseto, J. Kotek, B. Badet, P. Durand, E. Toth, *Chem. Eur. J.* **2012**, *18*, 1408–1418.
[18] J. F. He, C. S. Bonnet, S. V. Eliseeva, S. Lacerda, T. Chauvin, P. Retailleau, F. Szeremeta, B. Badet, S. Petoud, E. Toth, P. Durand, *J. Am. Chem. Soc.* **2016**, *138*, 2913–2916.
[19] K. Mason, N. J. Rogers, E. A. Suturina, I. Kuprov, J. A. Aguilar, A. S. Batsanov, D. S. Yufit, D. Parker, *Inorg. Chem.* **2017**, *56*, 4028–4038.
[20] J. A. Peters, K. Djanashvili, C. F. G. C. Geraldes, C. Platas-Iglesias, in *The Chemistry of Contrast Agents in Medical Magnetic Resonance Imaging* (Eds.: A. E. Merbach, L. Helm, E. Toth), Wiley-VCH., **2013**, pp. 209–276.
[21] F. Benetollo, G. Bombieri, L. Calabi, S. Aime, M. Botta, *Inorg. Chem.* **2003**, *42*, 148–157.
[22] M. Briganti, E. Lucaccini, L. Chelazzi, S. Ciattini, L. Sorace, R. Sessoli, F. Totti, M. Perfetti, *J. Am. Chem. Soc.* **2021**, *143*, 8108–8115.
[23] I. Lukeš, J. Kotek, P. Vojtíšek, P. Hermann, *Coord. Chem. Rev.* **2001**, *216–217*, 287–312.
[24] A. Spek, *Acta Crystallogr. Sect. D* **2009**, *65*, 148–155.
[25] C. F. Macrae, P. R. Edgington, P. McCabe, E. Pidcock, G. P. Shields, R. Taylor, M. Towler, J. van de Streek, *J. Appl. Crystallogr.* **2006**, *39*, 453–457.
[26] Y. Bretonnière, M. Mazzanti, J. Pécaut, F. A. Dunand, A. E. Merbach, *Inorg. Chem.* **2001**, *40*, 6737–6745.
[27] N. Chatterton, C. Gateau, M. Mazzanti, J. Pécaut, A. Borel, L. Helm, A. Merbach, *Dalton Trans.* **2005**, 1129–1135.
[28] E. Toth, R. Kiraly, J. Platzek, B. Raduchel, E. Brucher, *Inorg. Chim. Acta* **1996**, *249*, 191–199.
[29] R. Delgado, J. J. R. F. Da Silva, *Talanta* **1982**, *29*, 815–822.
[30] K. Kumar, C. A. Chang, L. C. Francesconi, D. D. Dischino, M. F. Malley, J. Z. Gougoutas, M. F. Tweedle, *Inorg. Chem.* **1994**, *33*, 3567–3575.
[31] A. Rodríguez-Rodríguez, Z. Garda, E. Ruscsák, D. Esteban-Gómez, A. de Blas, T. Rodríguez-Blas, L. M. P. Lima, M. Beyler, R. Tripier, G. Tircsó, C. Platas-Iglesias, *Dalton Trans.* **2015**, *44*, 5017–5031.
[32] M. Regueiro-Figueroa, B. Bensenane, E. Ruscsák, D. Esteban-Gómez, L. J. Charbonnière, G. Tircsó, I. Tóth, A. d. Blas, T. Rodríguez-Blas, C. Platas-Iglesias, *Inorg. Chem.* **2011**, *50*, 4125–4141.
[33] A. Takács, R. Napolitano, M. Purgel, A. C. Bényei, L. Zékány, E. Brücher, I. Tóth, Z. Baranyai, S. Aime, *Inorg. Chem.* **2014**, *53*, 2858–2872.
[34] M. Regueiro-Figueroa, E. Ruscsák, L. Fra, G. Tircsó, I. Tóth, A. de Blas, T. Rodríguez-Blas, C. Platas-Iglesias, D. Esteban-Gómez, *Eur. J. Inorg. Chem.* **2014**, *2014*, 6165–6173.
[35] R. Uzal-Varela, A. Rodríguez-Rodríguez, H. Wang, D. Esteban-Gómez, I. Brandariz, E. M. Gale, P. Caravan, C. Platas-Iglesias, *Coord. Chem. Rev.* **2022**, *467*, 214606.
[36] E. Szilagyi, E. Toth, Z. Kovacs, J. Platzek, B. Raduchel, E. Brucher, *Inorg. Chim. Acta* **2000**, *298*, 226–234.
[37] W. Cacheris, S. K. Nickle, A. D. Sherry, *Inorg. Chem.* **1987**, *26*, 958–960.
[38] Z. Baranyai, Z. Palinkas, F. Uggeri, A. Maiocchi, S. Aime, E. Brucher, *Chem. Eur. J.* **2012**, *18*, 16426–16435.
[39] E. Toth, E. Brucher, I. Lazar, I. Toth, *Inorg. Chem.* **1994**, *33*, 4070–4076.
[40] Z. Piskula, I. Svobodová, P. Lubal, S. Lis, Z. Hnatejko, P. Hermann, *Inorg. Chim. Acta* **2007**, *360*, 3748–3755.
[41] L. Burai, R. Király, I. Lázár, E. Brücher, *Eur. J. Inorg. Chem.* **2001**, *2001*, 813–820.
[42] E. Toth, L. Helm, A. Merbach, in *The Chemistry of Contrast Agents in Medical Magnetic resonance Imaging*, Second Edition ed. (Eds.: A. Merbach, L. Helm, E. Toth), John Wiley & Sons, Chichester, **2013**, pp. 25–81.
[43] R. Ruloff, E. Toth, R. Scopelliti, R. Tripier, H. Handel, A. E. Merbach, *Chem. Commun.* **2002**, 2630–2631.
[44] E. Toth, L. Burai, E. Brucher, A. E. Merbach, *J. Chem. Soc. Dalton Trans.* **1997**, 1587–1594.
[45] A. Nucera, C. Platas-Iglesias, F. Carniato, M. Botta, *Dalton Trans.* **2023**, *52*, 17229–17241.
[46] O. V. Yazyev, L. Helm, V. G. Malkin, O. L. Malkina, *J. Phys. Chem. A* **2005**, *109*, 10997–11005.

[47] A. Borel, S. Laus, A. Ozarowski, C. Gateau, A. Nonat, M. Mazzanti, L. Helm, *J. Phys. Chem. A* **2007**, *111*, 5399–5407.
[48] D. H. Powell, O. M. Ni Dhubhghaill, D. Pubanz, Y. Lebedev, W. Schlaepfer, A. E. Merbach, *J. Am. Chem. Soc.* **1996**, *118*, 9333–9346.
[49] H. M. Irving, M. G. Miles, L. D. Pettit, *Anal. Chim. Acta* **1967**, *38*, 475–488.
[50] L. Zékany, I. Nagypal, in *Computational Methods for the Determination of Formation Constants* (Ed.: D. J. Leggett), Plenum Press, New York, **1985**, p. 291.
[51] O. D. Rigaku, *CrysAlis PRO. Rigaku Oxford Diffraction*, **2015**, Yarnton, Oxfordshire, England.
[52] R. W. W. Nonius-Hooft, *COLLECT. Nonius BV*, **1998**, Delft, The Netherlands.
[53] Z. Otwinowski, W. Minor, *Methods Enzymol.* **1997**, *276*, 307–326.
[54] G. M. Sheldrick, *Acta Crystallogr.* **2015**, *C71*, 3–8.
[55] G. M. Sheldrick *Acta Crystallogr.* **2008**, *A64*, 112–122.
[56] G. M. Sheldrick, *Acta Crystallogr.* **2015**, *A71*, 3–8.
[57] S. Parsons, H. D. Flack, T. Wagner, *Acta Crystallogr.* **2013**, *B69*, 249–259.
[58] A. Spek, *Acta Crystallogr.* **2009**, *D65*, 148–155.
[59] C. F. Macrae, P. R. Edgington, P. McCabe, E. Pidcock, G. P. Shields, R. Taylor, M. Towler, J. van de Streek, *J. Appl. Crystallogr.* **2006**, *39*, 453–457.
[60] P. Urbanovský, J. Kotek, I. Císařová, P. Hermann, *Dalton Trans.* **2020**, *49*, 1555–1569.
[61] P. Urbanovský, J. Kotek, F. Carniato, M. Botta, P. Hermann, *Inorg. Chem.* **2019**, *58*, 5196–5210.

Manuscript received: December 22, 2023
Revised manuscript received: January 17, 2024
Accepted manuscript online: January 17, 2024
Version of record online: January 30, 2024